Journal of Computational Applied Mechanics 2024, 55(4): 605-616
DOI: 10.22059/JCAMECH.2024.374727.1029

RESEARCH PAPER

An investigation into the numerical analysis of refined higher order shear deformation theory for frequency responses of two-directional functionally graded taper beams

G. Chandra Mohana Reddy [a,1], Ch Ravikiran [a], S Nagaraju [a], P. Bridjesh[b]

[a] *Department of Mechanical Engineering, MLR Institute of Technology, Hyderabad, India*
[b] *Department of Chemical & Materials Engineering, College of Science, Engineering and Technology, University of South Africa (UNISA), c/o Christiaan de Wet & Pioneer Avenue, Florida Campus 1710, Johannesburg, South Africa*

Abstract

The study analyzes functionally graded (FG) beams' behavior with two-directional tapers, incorporating porosity effects and a Winkler-Pasternak elastic foundation. The analysis reveals that porosity reduces the beam's stiffness and natural frequencies while increasing the gradient index, which enhances its vibrational performance. The study also highlights the importance of the taper ratio in determining the beam's vibrational characteristics. This research provides a foundation for designing advanced structural elements in engineering applications.

Keywords: Winkler-Pasternak foundation. Functionally graded materials. Taper Beam. Free vibration;

1. Introduction

An essential aspect of developing structural design and guaranteeing structural integrity is the examination of the vibration properties of Two-directional Functionally Graded Porous Taper Beam (TDFGPTB) using refined higher-order shear deformation theory (RHSDT). Understanding of the dynamic characteristics exhibited by Functionally Graded Materials (FGM) within tapered beam structures facilitates the enhancement of material gradients and leads to progress in various engineering domains such as heat shields in aircraft, fusion reactors, heat exchangers, turbine blades, etc. in which the material experiences a significantly elevated temperature field characterized by a substantial temperature gradient both on the surface and inside its thickness[1].

Intricate structural components encounter dynamic loads that result in vibration. In some instances, the magnitude of dynamic loading might be sufficiently intense to result in significant deformations, hence introducing complexity to the system via the induction of geometric nonlinearity. FGMs have attracted considerable interest in the structural engineering field owing to their distinctive characteristics, which exhibit continuous variation throughout their volume[2]. Stress concentrations in homogeneous materials may cause early failure under specific loading circumstances, while FGMs may improve load-bearing and stress distribution by gradually changing their material composition.

Previous research has examined many aspects of vibration analysis in functionally graded taper beams (FGTB), providing significant contributions to understand their dynamic characteristics and structural performance. conducted a comparative analysison the effectiveness of 1D and 3D models in modeling free vibrations of FGTBs using ABAQUS and found that as FGTB geometric complexity and material inhomogeneity increase, the differences between models become more noticeable[3]. conducted a comparative analysis of deflections in a FGTB undera uniformly distributed load using the higher-order shear deformation theory (HSDT), power-law formula, Hamilton's principle, and Navier's solutions and concluded that the geometrical factors influence the structural analysis of the beam[4]. used HSDT and von-Kármán's nonlinear geometric relation to create linear and nonlinear iso-geometric finite element models for an FGTB with graphene platelet-reinforced composite and the nonlinear bending and vibration responses were examined through parametric studies[5]. Explored the relationship between size and nonlinear free longitudinal vibration of axially functionally graded nanorods using nonlocal elasticity theory while using Hamilton's principle to compute nonlinear natural frequencies[6].

conducted a numerical study on dimensionless natural frequencies of non-uniform aluminum beams covered with FGM and found that the width of the beams exhibits variability, coating material's characteristics change according to a polynomial function and highlighted the importance of considering the critical threshold for shape variation[7]. investigated the vibrations of a cantilevered conical beam, focusing on the non-linear impacts of curvature and inertia on the frequency response using the Euler-Bernoulli beam theory and Hamiltonian mechanics principles and explored the influence of material distribution on the system's

[1]Corresponding author. Tel.: +91-8297909752; *E-mail address:* cmreddy115@gmail.com

frequency response during the early resonance stage, integrating finite gradient methodology and nonlinear dynamics[8]. studied the vibration mechanics of a porous bi-directional functionally graded doubly curved sandwich shell using HSDT theory and the p-version finite element technique and explored the impact of gradient indices and porosity distribution on performance[9]. conducted a nonlinear study on a cantilever bar element made of graded material with porosity characteristics, considering the axial orientation, material properties, and stress-strain relationship and found that porosity and material graduation significantly influenced the bar element's nonlinear behavior[10, 11].They developed a closed-form solution for frequency vibration, incorporating nonlocal parameters in Bessel functions and found that in-plane pre-loads significantly influence natural frequencies for decreasing radii of the circular nanoplate .

Various solution methods have been proposed for solving the governing equations that assess the vibration of Functionally Graded Beams (FGB). The primary objective of analytical approaches is to get precise solutions to the differential equations, considering simplifying assumptions and using closed-form solutions such as exact solutions as adapted by, typically based on Galerkin and state space formulation[12]. The method of initial values was adapted by to consider the small-scale effects occurring in structures of smaller size[13]. Solved the governing equation of motion for vibration analysis using the Galerkin method and parametric investigations have been conducted on elastic foundations to examine the outcomes and applicability to real-world issues and concluded that the varied foundation exerts a substantial impact on the FGM[14]. Studied the nonlinear behavior of a porous functionally graded Euler-Bernoulli nanobeam under mechanical and electrical loads using nonlocal strain gradient elasticity theory. They used Hamilton's principle, Galerkin techniques and other methods to solve governing equations for various boundary conditions. The findings revealed that length-scale characteristics significantly influence the nonlinear vibration behavior of these devices.

Conducted a study on the free vibration analysis of FGTB to observe the impact of shear strain and solved the governing equations using the complementary functions method[15]. proposed the generalized differential quadrature method (GDQM) for solving the governing equation and estimating the coefficients for assessing the structural mechanics of a Timoshenko nanobeam which is functionally graded and tapered[16]. GDQM was also used by in assessing the vibration analysis of a FGTB composed of piezoelectric material[17]. The iso-geometric analysis was adapted by in studying the vibration characteristics of curved microbeams. Utilizing numerical approaches, the beam domain is discretized using numerical methods, and the governing equations are solved by utilizing numerical methods[18]. used Fredholm integral equations to analyze the free vibration in a FGTB and studied the effect of axial force and shear deformation[19]. studied nanocomposite microbeams reinforced with FGTB, focusing on size-dependent free vibration and buckling characteristics and suggested that synchronized axial distributions could enhance buckling resistance and natural frequency, while used homogenization methodology to assess microbeam vibration mechanics[20, 21].Studied thermal-induced shear buckling of orthotropic single-layered graphene sheets using nonlocal elasticity theory and the differential quadrature method. They analyzed six border conditions, considering elastic media, temperature variations, material properties, and boundary conditions.

Used the Chebyshev-Ritz method to compute buckling and compared it with buckling tests on composites made from epoxy resin, glass fiber, and nanorods and found that nanorods enhance tensile strength, rigidity, and critical buckling load[22]. Studied a sandwich composite beam strengthened with carbon nanorods from potato waste that was subjected to axially variable force, and the behavior of the beam was analyzed using strain gradient, general strain theory, shear deformation theory and HSDT. They found that using recycled materials enhances sandwich beam rigidity and increase critical buckling loads[23]. Examined the stability of a spinning viscoelastic sandwich beam with a soft core and carbon nanotube reinforced metal matrix nanocomposites skin, focusing on residual stress effects and the governing equations of motion for a rotating viscoelastic sandwich beam. Factors such as carbon nanotube distribution, volume fraction, spinning speed, critical loading, core thickness, axial force, and residual stress were investigated and suggested that varying spinning speeds can determine the ideal core thickness to prevent instability[24].Studied the vibration characteristics of multilayered piezoelectric nanobeams using Timoshenko beam theory, nonlocal continuum theory, surface elasticity theory and the differential quadrature method.Studiedthe vibration behaviors of a micro-cylindrical sandwich panel using carbon nanotubes and graphene platelets as reinforcements with porous and foam cores and analyzed higher-order shear deformation theory. They found that natural frequencies decrease with temperature but increase with SMA materials. The impact of different core materials on sandwich composite plates' low velocity impact behavior, to design and manufacture samples with more stored energy against impact and to find light sandwich structures[25]. The method for synthesizing hollow magnetic spheres with antibacterial properties, which could be useful in medicine, particularly cancer treatment and a hydrothermal method for synthesizing carbon nano-arrays using locally available materials using stainless steel type 1.4401 for autoclave system construction[26, 27].

Studied the oscillation characteristics of a sandwich beam with a porous core and composite face layers with shape memory alloy (SMA) under free and forced vibrations. They used Vlasov's model, Hamilton's principle, first-order shear deformation theory, Navier's method and validated results using relevant literature sources, while the key variables included temperature, SMA volume fraction, porosity distribution, CNT weight fraction, and geometric factors[28, 29]. Analyzed the structural properties of a sandwich beam strengthened with carbon nanotubes/graphene origami auxetic metamaterials (GOAM) and porous cores. They used the variational iteration method (VIM) to solve the equations of motion under different boundary conditions. Factors such as carbon nanotube distribution, porosity coefficient, porous core type, porosity parameter, weight fraction, and GOAM folding degree were examined. The results showed a strong agreement with previous studies, with a maximum error percentage of 0.3% for the first five frequencies and 0.22% for the first frequency[30, 31]. The buckling, vibration and deflections in a five-layer sandwich nanocomposite beam, with reinforcements of graphene platelets (GPLs) and shape memory alloys (SMAs), and a foam core was investigated and the Coriolis effect on the vibration analysis was investigated[32]. Studied the oscillation characteristics of circular graphene sheets under in-plane pre-load.

Prior studies on vibration analysis in FGBs have made significant contributions to the comprehension of their dynamic properties and structural applicability. The findings of a comparative study indicate that there is an increasing variation in the geometric complexity along with material inhomogeneity of FGBs. Research has also investigated the deflections in FGBs when subjected to homogenous loads, with a focus on the impact of geometrical parameters on structural analysis. The assessment of FGB vibrations has been conducted using various kinds of solution techniques, including analytical, semi-analytical, and numerical approaches.

This research paper highlights a significant gap in existing literature, highlighting a lack of comprehensive exploration of free vibration characteristics in TDFGPTBs using RHSDT. This study aims to create a model of a TDFGPTB, extract the governing equation that describes the vibration characteristics of the TDFGPTB. This will be done by employing the displacement fields and stress-strain relations, which are based on Hooke's law. The solution to the governing equation will be achieved using the Ritz technique. The accuracy of the developed beam model is confirmed by comparing it with existing data in scientific literature, and further verified by considering both alumina and aluminum as potential materials for the beamto thoroughly investigate the behavior of free vibration in TDFGPTB, adapting RHSDT under different boundary conditions. Vibration analysis of TDFGPTB using RHSDT is essential for understanding the dynamic behavior of functionally graded taper beams, facilitating their design, analysis, and optimization in various engineering applications such as aerospace, automotive, civil structures, and biomedical devices.

2. Nomenclature

x, y, z	Different coordinates along length, width, thickness directions of beam
TD	Two dimensional
FGB	Functionally graded beam
SS	Simply supported
L	Length
K	Kinetic energy
h	Height
Vf	Volume fraction
Pz	Gradient index in thickness direction
Px	Gradient index in length direction
F(z)	Shear shape function
HSDT	Higher order shear deformation theory
E	Modulus of elasticity
μ	Poisson’s ratio
ρ	Mass density α coefficient of porosity
(z)	Shear shape function σx Axial stress τxz Shear stress
RHSDT	Refined higher-order shear deformation theory
U	Strain energy
c	Ceramic
m	Metal
n	Taperness parameter
TBT	Timoshenko beam theory

3. Material properties of TDFGPTB

The study favors TDFGPTBs due to their variation in composition, material parameters, and thickness. The non-uniform beams have h_2 and h_1 thicknesses, determined by the equation $h(x) = h_2 [1 - n(x/L)]$.

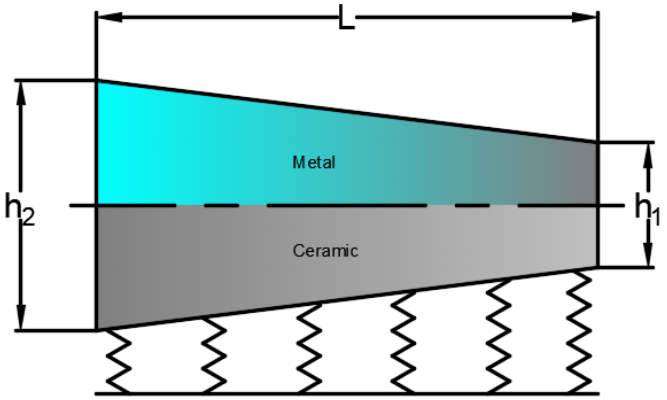

Fig1:Geometry of FG Taper Beam.

Fluctuations in the volume proportion of the component materials cause TDFGPTB properties to constantly fluctuate. Let's consider a functional correlation between the thickness coordinate and certain material properties as shown in Fig.2.The volume fraction of metal (V_m) can be mathematically represented using the power law equation [16].

$$V_f(x,z) = \left(\frac{x}{L}\right)^{px}\left(\frac{1}{2}+\frac{z}{h(x)}\right)^{pz} \quad (1)$$

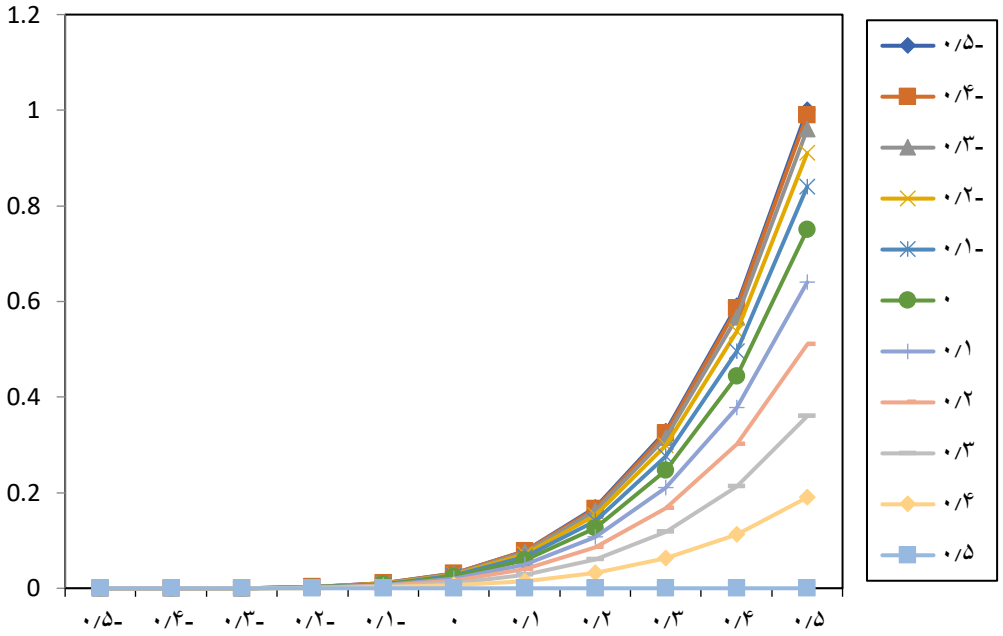

Fig 2: Metal volume fractions in the direction of length (x/L) and thickness (z/h)

3.1. TDFGPTB Formula

The assumption is that Young's modulus E and mass density ρ varies continuously along the thickness and length directions based on the volume percentages of constituents. Poisson's ratio μ is assumed to be fixed.

The following is a list of the TDFGPTB's density ("ρ"), Poisson's ratio ("μ"), and modulus of elasticity ("E") [16].

$$E(x,z) = (E_c - E_m)\left(\frac{z}{h(x)}+\frac{1}{2}\right)^{pz}\left(\frac{x}{L}\right)^{px} + E_m\text{-}\frac{\alpha}{2}(E_c + E_m) \quad (2)$$

$$\rho(x,z) = (\rho_c - \rho_m)\left(\frac{z}{h(x)}+\frac{1}{2}\right)^{pz}\left(\frac{x}{L}\right)^{px} + \rho_m\text{-}\frac{\alpha}{2}(\rho_m+\rho_c) \quad (3)$$

Material properties of beam, modulus elasticity 'E' and density 'ρ' of FGM porous beam (uneven) is given below

$$E(x,z) = (E_c - E_m)\left(\frac{z}{h(x)}+\frac{1}{2}\right)^{pz}\left(\frac{x}{L}\right)^{px} + E_m\text{-}\frac{\alpha}{2}(E_c + E_m)\left(1\text{-}\frac{2|z|}{h}\right) \quad (4)$$

$$\rho(x,z) = (\rho_c - \rho_m)\left(\frac{z}{h(x)}+\frac{1}{2}\right)^{pz}\left(\frac{x}{L}\right)^{px} + \rho_m\text{-}\frac{\alpha}{2}(\rho_m+\rho_c)\left(1\text{-}\frac{2|z|}{h}\right) \quad (5)$$

3.2 Motion-Governing Equations

Consider a FG beam consists of ceramic–metal resting on Winkler-Pasternak foundation, which has length, L; width b; andthickness, h, as shown in Fig1. Along with the refined shear deformation theory, displacements at any point of a FG beam can be expressed as follows.

$$u(x,z,t) = u_0(x,t) - z\frac{\partial w_b}{\partial x}(x,t) + f(z)\frac{\partial w_s}{\partial x} \quad (6)$$

$$w(x,z,t) = w_b(x,t) \quad (7)$$

In view of elastic constitutive law, normal stress can be stated as follows.

$$\sigma_x(x,z) = E(x,z)\varepsilon_x = E(x,z)\left(\frac{\partial u_0}{\partial x} - z\frac{\partial^2 w_b}{\partial x^2} + f(z)\left(\frac{\partial w_s}{\partial x}\right)\right) \quad (8)$$

$$\gamma_{xz} = g(z)\gamma_{xz}^s \quad (9)$$

$$\int_{t_1}^{t_2}(\delta U - \delta K)dt = 0 \quad (10)$$

$$\delta U = \int_0^L \int_{-\frac{h}{2}}^{\frac{h}{2}} (\sigma_x \delta\varepsilon_x + \tau_{xz}\delta\gamma_{xz})\, dxdz \quad (10a)$$

where N_x, M_x^b, M_x^s, and Q_{xz} are the material stress components of the FG beam and defined as follows

$$N_x, M_x^b, M_x^s = \int_0^l (1, z, f(z))\sigma_x dz \tag{11}$$

$$Q_{xz} = g(z)\tau_{xz} dz \tag{12}$$

The variation of the potential energy of Winkler-Pasternak model is presumed to be

$$\delta U_{wp} = \int_0^L \left[K_W(w_b + w_s)\delta(w_b + w_s) + K_p \frac{\partial^2(w_b+w_s)}{\partial x^2}\delta(w_b + w_s)\right] dx \tag{13}$$

where K_W and K_P are the transverse and shear stiffness coefficients of the foundation, respectively. as $k_P = 0$, the Winkler-Pasternak foundation reduces to the Winkler foundation.
The variation of the kinetic energy of Winkler-Pasternak model given by

$$\delta K = \int_0^L \{I_0\left[\frac{\partial u_0}{\partial x}\delta\frac{\partial u_0}{\partial x} + \left(\frac{\partial w_b}{\partial x} + \frac{\partial w_s}{\partial x}\right)\left(\delta\frac{\partial w_b}{\partial x} + \delta\frac{\partial w_s}{\partial x}\right)\right] - I_1\left(\frac{\partial u_0}{\partial x}\frac{d\delta\partial w_b}{dx} + \frac{d\partial w_b}{dx}\delta\frac{\partial u_0}{\partial x}\right) + I_2\left(\frac{d\partial w_b}{dx}\frac{d\delta\partial w_b}{dx}\right) + J_1\left(\frac{\partial u_0}{\partial x}\frac{d\delta\partial w_s}{dx} + \frac{d\partial w_s}{dx}\delta\frac{\partial u_0}{\partial x}\right) + K_2\left(\frac{d\partial w_s}{dx}\frac{d\delta\partial w_s}{dx}\right) + J_2\left(\frac{d\partial w_b}{dx}\frac{d\delta\partial w_s}{dx} + \frac{dw_s}{dx}\frac{d\delta\partial w_b}{dx}\right)\} \tag{14}$$

where dot-superscript convention indicates the differentiation with respect to the time variable t; and (I0, I1, J1, I2, J2, K2) are the mass inertias defined as

$$(I_0, I_1, J_1, I_2, J_2, K_2) = \int_0^L (1, z, f, z^2, zf, f^2)\,\rho(z) dz \tag{15}$$

Substituting the expressions for δU, δUef, δV and δT from Eqs. (13) and (14) into Eq. (10) and integrating the displacement gradients by parts and setting the coefficients of δu0, δwb and δws to zero separately, the following equations of motion are obtained:

$$\delta u_0 = \frac{dN_x}{dx} = I_0\frac{\partial^2 u_0}{\partial x^2} - I_1\frac{d\partial^2 w_b}{\partial x^2} + J_1\frac{d\partial^2 w_s}{\partial x^2} \tag{16}$$

$$\delta w_b = \frac{d^2 M_b}{dx^2} + q + K_p\left(\frac{d^2(w_b+w_s)}{\partial x^2}\right) - K_w(w_b + w_s) = I_0\left(\frac{\partial^2 w_b}{\partial x^2} + \frac{\partial^2 w_s}{\partial x^2}\right) + I_1\frac{\partial^2 u_0}{\partial x^2} - I_2\frac{d\partial^2 w_b}{\partial x^2} + J_2\frac{d\partial^2 w_s}{\partial x^2} \tag{16a}$$

$$\delta w_s = \frac{d^2 M_s}{dx^2} + \frac{dQ_{xz}}{dx} + q + K_p\left(\frac{d^2(w_b+w_s)}{\partial x^2}\right) - K_w(w_b + w_s) = I_0\left(\frac{\partial^2 w_b}{\partial x^2} + \frac{\partial^2 w_s}{\partial x^2}\right) + J_1\frac{\partial^2 u_0}{\partial x^2} - J_2\frac{d^2\partial^2 w_b}{\partial x^2} + K_2\frac{d^2\partial^2 w_s}{\partial x^2} \tag{16b}$$

Introducing Eqs. (11) and (12) into Eqs. (16)–(16b), the equations of motion can be expressed in terms of displacements (u_0, w_b,w_s) and the appropriate equations take the form;

$$A_{11}\frac{\partial^2 u_0}{\partial x^2} - B_{11}\frac{\partial^3 w_b}{\partial x^3} + B^s{}_{11}\frac{\partial^3 w_s}{\partial x^3} = I_0\frac{\partial^2 u_0}{\partial x^2} - I_1\frac{d\partial^2 w_b}{\partial x^2} + J_1\frac{d\partial^2 w_s}{\partial x^2} \tag{16c}$$

$$B_{11}\frac{\partial^3 u_0}{\partial x^3} - D_{11}\frac{\partial^4 w_b}{\partial x^4} + D^s{}_{11}\frac{\partial^4 w_s}{\partial x^4} + Q + K_p\left(\frac{d^2(w_b+w_s)}{dx^2}\right) - K_w(w_b + w_s) = I_0\left(\frac{\partial^2 w_b}{\partial x^2} + \frac{\partial^2 w_s}{\partial x^2}\right) + I_1\frac{\partial^2 u_0}{\partial x^2} - I_2\frac{d^2\partial^2 w_b}{\partial x^2} + J_2\frac{d^2\partial^2 w_s}{\partial x^2} \tag{17}$$

$$B^s{}_{11}\frac{\partial^3 u_0}{\partial x^3} - D^s{}_{11}\frac{\partial^4 w_b}{\partial x^4} + H^s{}_{11}\frac{\partial^4 w_s}{\partial x^4} + A^s{}_{55}\frac{\partial^2 w_s}{\partial x^2} + q + K_p\left(\frac{d^2(w_b+w_s)}{dx^2}\right) - K_w(w_b + w_s) = I_0\left(\frac{\partial^2 w_b}{\partial x^2} + \frac{\partial^2 w_s}{\partial x^2}\right) + J_1\frac{\partial^2 u_0}{\partial x^2} - J_2\frac{d^2\partial^2 w_b}{\partial x^2} + K_2\frac{d^2\partial^2 w_s}{\partial x^2} \tag{18}$$

where A11, D11, etc., are the beam stiffness, defined by

$$A_{ij}, A^s{}_{ij}, B_{ij}, D_{ij}, B^s{}_{i,j}, D^s{}_{ij}, H^s{}_{ij} = \int_0^L Q_{ij}(1, g^2(z), z, z^2, f(z)zf(z), f^2(z))dz \tag{19}$$

$$u_0(x,t) = \sum_{j=1,3,5}^{m} A_{j\theta_j}(x)e^{i\omega t}, \tag{20}$$

$$w_0(x,t) = \sum_{j=1,3,5}^{m} B_j\varphi_j(x)e^{i\omega t}, \tag{21}$$

$$\emptyset(x,t) = \sum_{j=1,3,5}^{m} C_{j\psi_j}(x)e^{i\omega t}, \tag{22}$$

Conditions at the boundaries are proposed $\theta_j(x)$,$\varphi_j(x)$ and $\psi_j(x)$ as the shape functions and $\boldsymbol{\omega}$ is the natural frequency of beam.

To use the complex number $i = \sqrt{-1}$ in determining unknown coefficients A_j, B_j, and C_j.

As a result of using qj to represent the values of Aj, Bj, andCj,

$$\begin{bmatrix} [S_{11}] & [S_{12}] & [S_{13}] \\ [S_{12}]^T & [S_{22}] & [S_{23}] \\ [S_{13}]^T & [S_{23}]^T & [S_{33}] \end{bmatrix} - \omega^2 \begin{bmatrix} [M_{11}] & [M_{12}] & [M_{13}] \\ [M_{12}]^T & [M_{22}] & [M_{23}] \\ [M_{13}]^T & [M_{23}]^T & [M_{33}] \end{bmatrix} \begin{Bmatrix} A \\ B \\ C \end{Bmatrix} = \begin{Bmatrix} \{0\} \\ \{0\} \\ \{0\} \end{Bmatrix} \tag{23}$$

$$S_{11} = A_{11}\alpha^2 \tag{24}$$

$$S_{12} = -B_{11}\alpha^3 \tag{24a}$$

$$S_{13} = B^{s}{}_{11}\alpha^3 \tag{25}$$

$$S_{22} = D_{11}\alpha^4 + K_W + K_p\alpha^2 \tag{26}$$

$$S_{23} = D^{s}{}_{11}\alpha^4 + K_W + K_p\alpha^2 \tag{27}$$

$$S_{33} = H^{s}{}_{11}\alpha^4 + A^{s}{}_{55}\alpha^2 + K_W + K_p\alpha^2 \tag{28}$$

$$M_{11} = I_0 \tag{29}$$

$$M_{12} = -I_1\alpha \tag{30}$$

$$M_{13} = -J_1\alpha \tag{31}$$

$$M_{22} = I_0 + I_2\alpha^2 \tag{32}$$

$$M_{23} = I_0 + J_2\alpha^2 \tag{33}$$

$$M_{33} = I_0 + K_2\alpha^2 \tag{34}$$

3. Results and discussion

The vibration behavior of TDFGPTB is influenced by factors such as taper ratio, aspect ratio, gradation exponents, and material property gradient. Increased taper ratios and decreased aspect ratios lead to intricate vibration patterns. Gradation exponents affect the speed of material properties variation within FGM layers. Higher gradation exponents and steep gradients result in significant variations in stiffness and mass distribution, causing vibration characteristics. Numerical studies predict static analyses with various boundary conditions.

Alumina:E_c=380 Gpa, $\rho_c = 3960\,\frac{\text{kg}}{\text{m}^3}$, μ_c= 0.3

Aluminum:E_m= 70 Gpa, $\rho_m = 2702\,\frac{\text{kg}}{\text{m}^3}$, μ_m= 0.3

Table 1:Numerical calculations based on kinematic boundary conditions (BC).

BC	x = -L/2	x = +L/2
SS	u =0, w=0	w =0

The characteristics of the TDFGPTB material fluctuate in axial (L) and thickness (h) directions, according to power-law distribution. The dimensionless frequency (λ) parameter is used to represent the results.

$$\lambda = \frac{\omega L^2}{h}\sqrt{\frac{\rho_m}{E_m}} \tag{35}$$

3.1. Validation

The selection of taper ratios, aspect ratios, and gradation exponents for beam analysis involves a balance between structural requirements, geometric constraints, numerical considerations, and the objectives of the study. These parameters play a crucial role in defining the geometry and behavior of the beams under investigation and are chosen thoughtfully to ensure the relevance and reliability of the analysis. For numerical analysis, it is assumed that the material properties of the beam are homogeneous throughout, the material behavior is linear, and the load is distributed uniformly to facilitate the present investigation. A thorough and meticulous validation of the TDFGPTB using RHSDT is performed using the non dimensional frequency as Eq. (35). Table 2 displays the results and comparisons based on idealized beams with various BCs. The current study's findings slightly deviate from those published by Shanab et al. [16]. For the SS beam, the frequency results in Table 3are also the same; the deviation is attributed to the fact that the present study deals with the RHSDT, in which the shear stress is made zero at the top and bottom surfaces of the beam for accuracy result, whereas Shanab et al. [16] theory was related to the TBT, in which the shear shape function and the shear factor couldn't be considered. The comparison of the RHSDT and TBT across different taper ratios yields essential insights into the vibrational characteristics of TDFGPTB. The RHSDT consistently estimates frequencies compared to TBT for all taper ratios. This variance arises from the RHSDTs accuracy, in considering deformation and rotary inertia effects, particularly evident in thick beams. For a taper ratio of 10, the frequency under RHSDT is 20.66, but the TBT frequency is 17.51. This signifies a notable divergence, suggesting that RHSDT more successfully reflects the increased stiffness provided by material gradation and tapering compared to TBT. The difference between RHSDT and TBT underscores the challenges faced by TBT when dealing with scenarios that feature taper ratios or beams with variations in materials throughout their structure. RHSDTs incorporation of higher order elements offers an insight into the behavior of beams in situations where the structures are not uniform in their composition. In real world applications and practical uses where beams are subjected to loads. Especially when the taper ratio plays a role in design considerations. Relying on the results provided by RHSDT would yield more dependable outcomes, for engineers and designers. It can also be observed that at taper ratios (0 and 0.5), the distinction between RHSDT and TBT is minimal, suggesting

that TBT remains a viable approximation for minor tapering. As the taper ratio escalates, the gap expands, underscoring the necessity for RHSDT in more intricate situations characterized by substantial geometric and material discrepancies.

Table 2.Comparison of natural frequency of TDFGPTB at taper ratio (n=0)

Theory	0	0.5	1	2	5	10
TBT	10.59	14.45	15.75	16.76	17.39	17.51
HSDT(Present)	12.49	17.05	18.58	19.77	20.52	20.66

Table 3 displays a comparison of the natural frequencies of SS beams with a taper ratio of 0.5, as ascertained by the RHSDT and TBT. Both RHSDT and TBT suggest that as the gradient indices (0 to 10, with increments of 0 to 10) go up in value there will be a rise in the frequency observed in the beam structure analysis results. This is because as the beam material changes from being metal to predominantly ceramic over increasing indices it becomes more rigid and hence has higher natural frequencies. The Young's modulus of the section significantly boosts the beam's ability to resist vibrations resulting in the increase in observed frequencies. RHSDT integrates higher-order shear deformation effects, providing a more precise representation of the stiffness and inertia fluctuations in FGMs. The difference highlights the necessity of employing RHSDT for beams exhibiting considerable material gradation, as TBT may excessively simplify the dynamic response.

Table 3.Comparison of natural frequency of TDFGPTB at taper ratio (n= 0.5)

Theory	0	0.5	1	2	5	10
TBT	12.89	14.45	15.75	16.76	17.39	17.51
HSDT(Present)	15.46	17.34	18.9	20.11	20.86	21.01

Table 4 elucidates the natural frequencies of TDFGPTBs under SS boundary conditions at a taper ratio of 0.0, as affected by the gradient indices Pz and Px.For a constant Px, an increase in Pz results in elevated frequencies. At Px=0, the frequency rises from 12.49 when Pz =0 to 18.23 when Pz = 10. This trend is ascribed to the shift from a metal-dominant to a ceramic-dominant composition in the thickness direction. Ceramics, possessing a higher modulus of elasticity, substantially enhance stiffness, hence increasing natural frequencies.The progressive stiffening over the beam's length diminishes distortion, hence improving the vibrational properties.SS boundary conditions permit rotational freedom at the supports, resulting in comparatively lower natural frequencies. The observed trends align with the anticipated behavior of SS beams over different material gradations.

Table 4. Natural frequency of TDFGPTB at taper ratio (n=0.0)

	P_x					
P_z	0	0.5	1	2	5	10
0	12.49	14.63	15.92	17.37	18.81	19.25
0.5	14.89	16.35	17.2	18.16	19.07	19.33
1	15.73	16.94	17.65	18.43	19.15	19.36
2	16.54	17.49	18.05	18.66	19.21	19.38
5	17.56	18.16	18.52	18.92	19.29	19.4
10	18.23	18.61	18.84	19.91	20.15	20.22

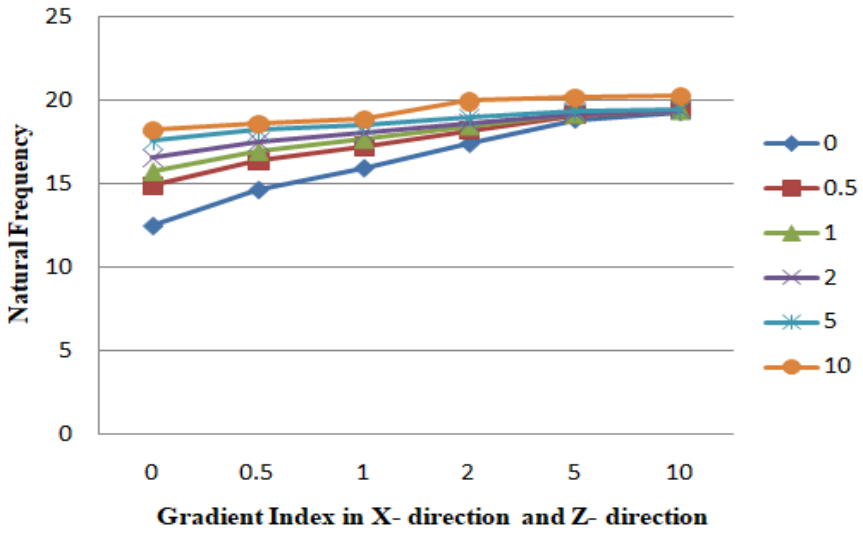

Fig 3: Natural Frequency of TDFGPTB at taper ratio (n= 0.0) in the direction of length (x/L) and thickness (z/h)

Table 5 displays the natural frequencies of TDFGPTBs under SS boundary conditions with a taper ratio of 0.5, affected by the gradient indices Pz and Px.For a constant Pz, the natural frequency increases with the rise in Px. For instance: At Pz=0, the frequency escalates from 15.46 at Px=0 to 23.76 at Px=10. This rise results from improved stiffness in the longitudinal direction as Px alters the beam's material composition from metal to ceramic, which exhibits greater stiffness and deformation resistance.The gradation in thickness substantially influences stiffness and mass distribution, enhancing vibrational resistance. The sensitivity of natural frequency to Pz is more pronounced at lower levels of Px, as longitudinal material gradation prevails at elevated Px. At elevated Pz and Px levels, the frequencies converge (e.g., 23.84–23.91 at Px=10), signifying saturation effects in the stiffness contributions due to material gradation.

Table 5. Natural frequency of TDFGPTB attaper ratio(n= 0.5)

	P_x					
P_z	0	0.5	1	2	5	10
0	15.46	18.34	19.98	21.76	23.34	23.76
0.5	18.39	20.34	21.43	22.58	23.58	23.78
1	19.41	21.04	21.94	22.86	23.66	23.81
2	20.4	21.68	22.39	23.11	23.73	23.88
5	21.64	22.46	22.92	23.4	23.8	23.9
10	22.47	22.98	23.27	23.58	23.84	23.91

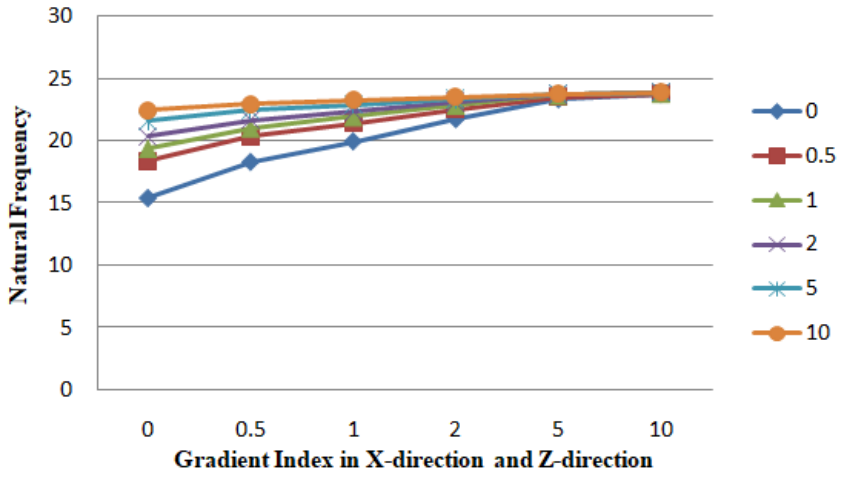

Fig 4: Natural Frequency of TDFGPTB at taper ratio (n= 0.5) in the direction of length (x/L) and thickness (z/h)

Table 6 demonstrates the variation of the fundamental natural frequency of TDFGPTB with respect to the gradient index (Pz) in the thickness direction and the porosity index. As the porosity index rises from 0 to 0.3, the natural frequency diminishes for all values of Pz. Porosity creates voids throughout the material, diminishing the effective stiffness and mass density of the beam. Reduced stiffness leads to diminished resistance to deformation, thereby decreasing the natural frequency.

Table 6. Natural frequency of TDFGPTB at taper ratio (n=0.5) and various gradient index under even porosity

	Porosity index			
P_z	0	0.1	0.2	0.3
0	15.46	15.27	14.97	14.49
0.5	15.43	14.82	14.01	13.63
1	15.36	14.67	13.89	13.27
2	15.21	14.39	13.53	12.97
5	14.39	14.05	13.21	12.46
10	14.17	13.89	13.05	12.18

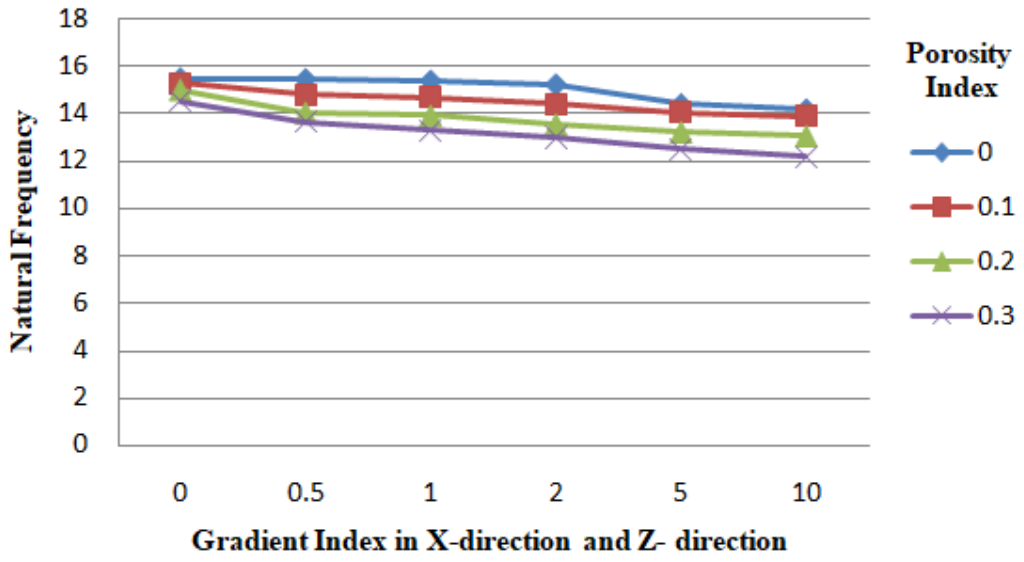

Fig 5: Natural frequency of TDFGPTB at taper ratio (n=0.5) and various gradient index under even porosity

Table 7 analyzes the variation in the fundamental natural frequency of TDFGPTB under non-uniform porosity circumstances, influenced by the *Pz* in the thickness direction and the porosity index. Irregular porosity results in non-uniform void distributions, affecting the beam's rigidity and vibrational properties. Irregular porosity results in areas of diminished material stiffness, causing localized decreases in stiffness and, therefore, lowered natural frequencies. The decrease is more gradual than that of equal porosity, as uneven void distribution may concentrate the effect. Elevated *Pz* values indicate a shift from a ceramic-dominant to a metal-dominant material composition. Metals exhibit less stiffness than ceramics, diminishing the beam's total rigidity and natural frequency. The interaction between *Pz* and the porosity index further diminishes the natural frequency. At elevated levels of both *Pz* and porosity index, the synergistic impact of diminished stiffness in material gradation and porosity is apparent. Irregular porosity results in somewhat elevated frequencies relative to uniform porosity for identical gradient and porosity indices. Irregular porosity does not consistently diminish stiffness across the beam, as voids are unevenly distributed. This localized stiffness retention partially alleviates the frequency drop.

Table 7. Fundamental natural frequency of TDFGPTB at various gradient index under un-even porosity

	Porosity index			
P_z	0	0.1	0.2	0.3
0	15.46	15.32	15.17	14.76
0.5	15.43	15.19	14.93	14.56
1	15.36	14.98	14.62	14.15
2	15.21	14.73	14.01	13.57
5	14.39	14.17	13.81	13.26
10	14.17	13.92	13.64	12.75

Table 2 compares the frequency results of RHSDT and TBT for SS beams, revealing that RHSDT has a higher frequency due to the use of a shear correction factor. The study found a higher error percentage when comparing results with [16], as [16] only used TBT in displacement direction without incorporating a shear correction factor. Table 3 shows that as the taper ratio increases, the frequency also rises, influenced by changing geometry.

Under SS boundary conditions, the suggested theory is applied to assess and compare the results of free vibration with those anticipated by a taper nano beam [16]. Satisfactory results are predicted by the presented theory. The remaining numbers, as shown in Table 5. Since the beam width is constant in this case, the applied load is constant along the length of the beam, but “moment of inertia” and “elastic modulus” vary with the beam length. The effects of the non-uniform parameter on the thickness variation, h(x), as well as the maximum dimensionless vibration at different power-law exponents and supporting types are discussed. The variation in the moment of inertia is caused by the change in thickness that takes place throughout the length of the beam. Table 4 and Table 6 show that the dimensionless frequency would rise for all types of supporting structures. Fig 3 and Fig 4 show that for SS beams and Fig 5 and Fig 6 show that the non-uniformity parameter reduces with *n*, however, the increase is dependent on the types of supporting elements.

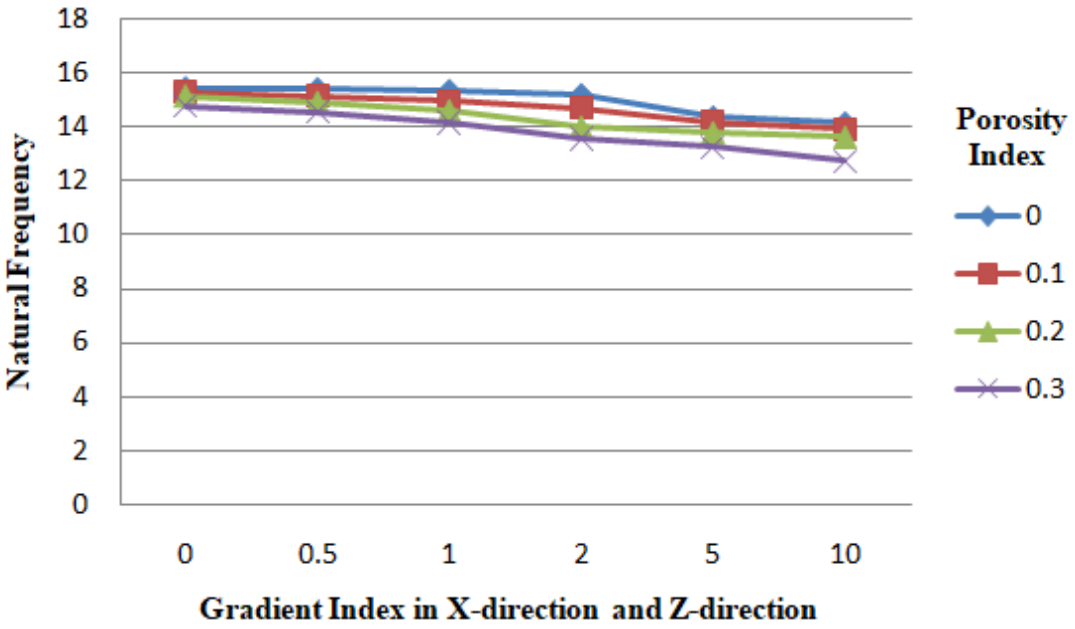

Fig 6: Natural frequency of TDFGPTB at taper ratio (n=0.5) and various gradient index under uneven porosity

Fig 3 indicates the frequency differences between the TBT and the RHSDT for the SS beam at zero taper. The frequency increases with an increase in the gradient indexes in the *x* and *z* directions because the beam is transformed from metal to ceramic. In ceramic, the young modulus is higher than in metal, so the ceramic is stiffer and tends to vibrate at higher frequencies. Fig. 4 indicates the frequency differences between the TBT and RHSDT for the SS beam at 0.5 taper. The frequency increases with an increase in the gradient indexes in the *x* and *z* directions because the beam converts from metal to ceramic. In ceramic, the young modulus is higher than in metal so the ceramic is stiffer and tends to vibrate at higher frequencies. Fig 5 indicates the frequency at RHSDT for the SS beam at zero taper. The frequency increases with an increase in the gradient indexes in the *x* and *z* directions because the beam converts from metal to ceramic. In ceramic, the young modulus is higher than in metal, so the ceramic is stiffer and tends to vibrate at higher frequencies. Fig 6 indicates the frequency at RHSDT for the SS beam at 0.5 taper ratio. The frequency increases with an increase in the gradient indexes in the *x* and *z* directions because the beam converts from metal to ceramic. In ceramic, the young modulus is higher than in metal, so the ceramic is stiffer and tends to vibrate at higher frequencies. As Table 4, the SS beam shows the highest rate of dimensionless frequency. The taper ratio of a TDFGPTB can lead to changes in the distribution of mass and stiffness along the length of the beam. This alteration can affect the natural frequencies of vibration modes. Higher taper ratios generally result in higher frequency responses due to the concentration of mass/stiffness towards one end of the beam. The aspect ratio (length-to-width ratio) of the beam can influence its bending behavior. For slender beams (high aspect ratios), higher frequency responses are typically observed due to the dominance of bending deformation modes. However, extremely high aspect ratios might introduce buckling instability, which can affect the frequency responses differently.

In contrast to the effects of thickness variation and the combination of thickness variation and width variation, where it has the greatest effects, the effects of width variation on the vibration in the beam are often not significant. Reducing the non-uniformity parameters implies that variances are causing the dimensionless vibration to rise. An SS beam experiences a rise in dimensionless vibration in addition to a change in the maximum dimensionless vibration's position due to the impacts of width variation, thickness variation, and both width and thickness variation. Variations in thickness as well as width contribute to an increase in dimensionless vibration. In most situations, the mid-span of an SS beam corresponds to the point of maximum vibration (i.e., x = l/2). It appears that both variations in the elastic modulus distribution and variations in the beam size cause the position of the dimensionless vibration to vary.

The introduction of a RHSDT for studying the vibration behavior of TDFGPTB resulted in the presence of computational complexity. The incorporation of higher-order elements required a more complex formulation and technique for finding a solution. In order to tackle this difficulty, rigorous validation and verification procedures were carried out to guarantee the precision of the numerical implementation. Ensuring the satisfaction of boundary conditions posed challenges, particularly in formulating admissible functions to meet the prescribed constraints. The incorporation of Ritz-type solutions using algebraic polynomials facilitated the fulfillment of boundary conditions in both directions, while convergence studies were conducted to validate the chosen boundary conditions and ensure their consistency with physical principles.

4. Conclusions

The free vibration analysis of functionally graded beams with two-directional taper, porosity, and a Winkler-Pasternak elastic foundation highlights the interplay of material and geometric properties in influencing dynamic performance. The study concludes that porosity significantly impacts the beam's stiffness and natural frequencies, reducing its overall rigidity. In contrast, increasing the gradient index enhances the beam's vibrational characteristics, demonstrating the effectiveness of tailored material grading.

The taper ratio is identified as a critical parameter that governs the mass and stiffness distribution, thereby influencing the natural frequencies and mode shapes. Furthermore, the Winkler-Pasternak foundation contributes to vibration control and stability, with foundation stiffness playing a pivotal role. These findings provide valuable insights for optimizing the design and performance of advanced structural elements in engineering applications.

- When a beam rests on a Winkler-Pasternak foundation, its natural frequency generally increases compared to a beam without foundation support.
- The foundation provides additional stiffness due to its elastic reactions, described by the Winkler (vertical support) and Pasternak (shear interaction) parameters.
- These parameters reduce beam deformation and enhance its vibrational stability.
- The magnitude of frequency change depends on the foundation's stiffness, the beam's material gradation, and boundary conditions. In some cases, excessive foundation stiffness may lead to non-linear frequency behavior.

References

[1] G. P. Sinha, B. Kumar, Review on vibration analysis of functionally graded material structural components with cracks, *Journal of Vibration Engineering & Technologies*, Vol. 9, pp. 23-49, 2021.

[2] P. Bridjesh, N. K. Geetha, B. Yelamasetti, Numerical investigation on buckling of two-directional porous functionally graded beam using higher order shear deformation theory, *International Journal on Interactive Design and Manufacturing (IJIDeM)*, pp. 1-14, 2023.

[3] V. Burlayenko, R. Kouhia, S. Dimitrova, One-dimensional vs. three-dimensional models in free vibration analysis of axially functionally graded beams with non-uniform cross-sections, *Mechanics of Composite Materials*, pp. 1-20, 2024.

[4] G. Reddy, P. Bridjesh, B. Reddy, K. Reddy, Comparison of Deflection in Two-Directional Functionally Graded Tapered Beam, *Mechanics of Advanced Composite Structures*, Vol. 11, No. 1, pp. 191-202, 2024.

[5] Y. Liang, S. Zheng, H. Wang, D. Chen, Nonlinear isogeometric analysis of axially functionally graded graphene platelet-reinforced composite curved beams, *Composite Structures*, Vol. 330, pp. 117871, 2024.

[6] R. Nazemnezhad, A semi analytical nonlinear approach for Size-dependent analysis of longitudinal vibration in terms of axially functionally graded nanorods, *Mechanics of Advanced Composite Structures*, 2024.

[7] H. Pekel, E. Erdurcan, Determination of natural frequencies of non-uniform aluminum beams coated with functionally graded material, *Materialwissenschaft und Werkstofftechnik*, Vol. 55, No. 2, pp. 204-215, 2024.

[8] R. Moalefshahri, Nonlinear vibrations of a cantilevered conical beam with axially functionally graded material carrying a longitudinally loaded mass, *Mechanics Based Design of Structures and Machines*, pp. 1-11, 2024.

[9] Z. Lakhdar, S. M. Chorfi, S. A. Belalia, K. M. Khedher, A. E. Alluqmani, A. Tounsi, M. Yaylacı, Free vibration and bending analysis of porous bi-directional FGM sandwich shell using a TSDT p-version finite element method, *Acta Mechanica*, pp. 1-30, 2024.

[10] Ş. D. Akbaş, Material Nonlinear Static Analysis of Axially Functionally Graded Porous Bar Elements, *Journal of Computational Applied Mechanics*, 2024.

[11] K. Hosseini-Hashemi, R. Talebitooti, S. Hosseini-Hashemi, R. Nazemnezhad, A unique and comprehensive approach to investigate the transverse free vibration of non-uniform and functionally graded Euler–Bernoulli beams, *Journal of the Brazilian Society of Mechanical Sciences and Engineering*, Vol. 45, No. 10, pp. 551, 2023.

[12] P. Elyasi, B. N. Neya, A. R. Firoozjaee, Free vibration of viscoelastic nonlocally damped tapered axially functionally graded beams using the state-space formulation, *Engineering Structures*, Vol. 288, pp. 116183, 2023.

[13] E. Demirkan, M. Çelik, R. Artan, Slope Deflection Method in Nonlocal Axially Functionally Graded Tapered Beams, *Applied Sciences*, Vol. 13, No. 8, pp. 4814, 2023.

[14] V. Kumar, S. Singh, V. Saran, S. Harsha, Vibration response analysis of tapered porous FGM plate resting on elastic foundation, *International Journal of Structural Stability and Dynamics*, Vol. 23, No. 02, pp. 2350024, 2023.

[15] T. A. Aslan, A. R. Noori, B. Temel, An efficient approach for free vibration analysis of functionally graded sandwich beams of variable cross-section, in *Proceeding of*, Elsevier, pp. 105397.

[16] R. A. Shanab, M. A. Attia, On bending, buckling and free vibration analysis of 2D-FG tapered Timoshenko nanobeams based on modified couple stress and surface energy theories, *Waves in Random and Complex Media*, Vol. 33, No. 3, pp. 590-636, 2023.

[17] B. Gupta, P. Sharma, S. Rathore, Free vibration analysis of AFGPM non-uniform beam: A mathematical modeling, *Journal of Vibration Engineering & Technologies*, Vol. 11, No. 7, pp. 2945-2954, 2023.

[18] S. Mirzaei, M. Hejazi, R. Ansari, Isogeometric analysis of small-scale effects on the vibration of functionally graded porous curved microbeams based on the modified strain gradient elasticity theory, *Acta Mechanica*, Vol. 234, No. 10, pp. 4535-4557, 2023.

[19] M. Mohammadnejad, Free vibration analysis of axially functionally graded beams using Fredholm integral equations, *Archive of Applied Mechanics*, Vol. 93, No. 3, pp. 961-976, 2023.

[20] D. Liu, J. Su, L. Zhao, X. Shen, State-Space Formulation for Buckling and Free Vibration of Axially Functionally Graded Graphene Reinforced Nanocomposite Microbeam under Axially Varying Loads, *Materials*, Vol. 17, No. 6, pp. 1296, 2024.

[21] K. Yee, O. Z. S. Ong, M. H. Ghayesh, M. Amabili, Various homogenisation schemes for vibration characteristics of axially FG core multilayered microbeams with metal foam face layers based on third order shear deformation theory, *Applied Mathematical Modelling*, Vol. 125, pp. 189-217, 2024.

[22] F. Bargozini, M. Mohammadimehr, The theoretical and experimental buckling analysis of a nanocomposite beams reinforced by nanorods made of recycled materials, *Polymer Composites*, Vol. 45, No. 4, pp. 3327-3342, 2024.

[23] F. Bargozini, M. Mohammadimehr, E. A. Dawi, M. Salavati-Niasari, Buckling of a sandwich beam with carbon nano rod reinforced composite and porous core under axially variable forces by considering general strain, *Results in Engineering*, pp. 101945, 2024.

[24] A. A. Monajemi, M. Mohammadimehr, Stability analysis of a spinning soft-core sandwich beam with CNTs reinforced metal matrix nanocomposite skins subjected to residual stress, *Mechanics Based Design of Structures and Machines*, Vol. 52, No. 1, pp. 338-358, 2024.

[25] A. Amiri, M. Mohammadimehr, M. I. Rahaghi, Vibration analysis of a micro-cylindrical sandwich panel with reinforced shape-memory alloys face sheets and porous core, *The European Physical Journal Plus*, Vol. 136, No. 8, pp. 887, 2021.

[26] M. Charekhli-Inanllo, M. Mohammadimehr, The effect of various shape core materials by FDM on low velocity impact behavior of a sandwich composite plate, *Engineering Structures*, Vol. 294, pp. 116721, 2023.

[27] A. Farazin, M. Mohammadimehr, H. Naeimi, F. Bargozini, Design, fabrication, and evaluation of green mesoporous hollow magnetic spheres with antibacterial activity, *Materials Science and Engineering: B*, Vol. 299, pp. 116973, 2024.

[28] A. Farazin, M. Mohammadimehr, H. Naeimi, Flexible self-healing nanocomposite based gelatin/tannic acid/acrylic acid reinforced with zinc oxide nanoparticles and hollow silver nanoparticles based on porous silica for rapid wound healing, *International Journal of Biological Macromolecules*, Vol. 241, pp. 124572, 2023.

[29] F. Bargozini, M. Mohammadimehr, E. A. Dawi, R. Monsef, Z. Heydariyan, M. Salavati-Niasari, Development and performance analysis of a 316 stainless steel autoclave for facile fabrication of carbon nanoarchitectures derived from natural potato and starch, *Journal of Materials Research and Technology*, Vol. 23, pp. 3126-3136, 2023.

[30] K. Alambeigi, M. Mohammadimehr, M. Bamdad, T. Rabczuk, Free and forced vibration analysis of a sandwich beam considering porous core and SMA hybrid composite face layers on Vlasov's foundation, *Acta Mechanica*, Vol. 231, pp. 3199-3218, 2020.

[31] M. K. Mogehi, M. Mohammadimehr, N. D. Duc, Vibration analysis of a sandwich Timoshenko beam reinforced by GOAM/CNT with various boundary conditions using VIM, *Materials Science and Engineering: B*, Vol. 304, pp. 117364, 2024.

[32] M. Arabzadeh-Ziari, M. Mohammadimehr, E. Arabzadeh-Ziari, M. Asgari, Deflection, buckling and vibration analyses for a sandwich nanocomposite structure with foam core reinforced with GPLs and SMAs based on TSDBT, *Journal of Computational Applied Mechanics*, Vol. 55, No. 2, pp. 289-321, 2024.